Rotation of a Charged Spin Probe in Room-Temperature Ionic Liquids

Jakov Slade,[a] Dalibor Merunka,[a] Ezequiel Huerta,[b] and Miroslav Peric [b,*]

[a] *Division of Physical Chemistry, Ruđer Bošković Institute, Bijenička cesta 54, HR-10000 Zagreb, Croatia*

[b]*Department of Physics and Astronomy and The Center for Biological Physics, California State University, Northridge Northridge, CA 91330*

Email: Miroslav.peric@csun.edu

ABSTRACT

X-band electron paramagnetic resonance spectroscopy has been used to investigate the rotational diffusion of a stable, positively charged nitroxide 4-trimethylammonium-2,2,6,6-tetramethylpiperidine-1-oxyl iodide (Cat-1) in a series of 1-alkyl-3-methylimidazolium tetrafluoroborate room temperature ionic liquids (RTILs) having alkyl chain lengths from two to eight carbons. The rotation of Cat-1 is anisotropic with the preferential axis of rotation along the NO˙ moiety. The Stokes−Einstein−Debye law describes the mean rotational correlation time of Cat-1, assuming that the hydrodynamic radius is smaller than the van der Waals radius of the probe. This implies that the probe rotates freely, experiencing slip boundary condition, which is solvent-dependent. The rotational correlation time of Cat-1 in RTILs can very well be fitted to a power-law functionality with a singular temperature, which suggests that the apparent activation energy of rotation exhibits non-Arrhenius behavior. Compared to the rotation of perdeuterated 2,2,6,6-tetramethyl-4-oxopiperidine-1-oxyl (pDTO), which is neutral, the rotation of Cat-1 is several times slower. The rotational anisotropy, the ratio of the rotational times of pDTO and Cat-1, and the apparent activation energy indicate the transition from a homogeneously globular structure to a sponge-like structure when the alkyl chain has four carbons, which is also observed in molecular dynamics computational studies. For the first time, we have been able to show that the rotational correlation time of a solute molecule can be analyzed in terms of the Cohen–Turnbull free volume theory. The Cohen-Turnbull theory fully describes the rotation of Cat-1 in all ionic liquids in the measured temperature range.

INTRODUCTION

Recently, room-temperature ionic liquids (RTILs) have garnered a lot of academic and industrial interests.[1-6] The reason is that these organic salts, which commonly melt below 100 ^{O}C and are made up of a great variety of asymmetric organic cations and organic or inorganic anions, have tunable physicochemical properties. Due to their tunability, RTILs can be used in many applications such as energy production and storage,[7] organic catalysis and synthesis,[8] separation technology,[9] and analytical chemistry.[10] RTILs are also seen as better alternatives to volatile organic solvents because of their negligible vapor pressure, low flammability, and their "green" nature.[9, 11] To use the full potential of RTILs as solvents for the reaction, it is necessary to study the solvation of solutes dissolved in RTILs.[2] Since the rotational diffusion of a solute molecule is affected by its solvation, and it has been common to study the solute solvation in RTILs by studying the rotational diffusion of fluorescent probes[12-14] and spin probes[15-17] dissolved in RTILs. NMR spectroscopy can also be used to study the solvation of solutes in RTILs.[18-20]

Nitroxides are useful spin probes because their electron paramagnetic resonance (EPR) spectra not only give information on their own dynamic behavior, but also through their interactions with the surroundings, they give a wealth of information about their environment.[21-22] Stable nitroxide probes, both charged and neutral, have often been used to study the rotational and translational dynamics of solutes in RTILs.[16-17, 23-32] The positively charged nitroxide 4-trimethylammonium-2,2,6,6-tetramethylpiperidine-1-oxyl iodide (Cat-1) has been used to understand the solvation and rotational dynamics of positively charged solutes in RTILs.[15, 17, 25, 33-34]

Using pulsed high-field W-band EPR spectroscopy and continuous wave X-band EPR, Akdogan *et al.*[15] have studied the solvation of three Tempo (2,2,6,6-tetramethylpiperidine-1-oxyl) based spin probes (4-carboxylate-Tempo, 4-hydroxy-Tempo or Tempol, and Cat-1) in imidazolium-based RTILs with different alkyl chain lengths (C_2 to C_6) with tetrafluoroborate (BF_4^-) and hexafluorophosphate (PF_6^-) anions. The chosen spin probes represented positively charged (Cat-1), negatively charged (4-carboxylate-Tempo), and neutral (Tempol) solutes. The charged probes experienced anisotropic rotational diffusion with the preferred axis of rotation along the $NO^{\cdot}$ moiety, while Tempol undergoes isotropic rotational diffusion. The changes of g_{xx} (x principal value of the g-tensor) and A_{zz} (z principal value of the hyperfine tensor) indicated that the charged side groups of Cat-1 and 4-carboxylate-Tempo interact electrostatically with the charged parts of the RTILs. Cat-1 seems to reside in the polar region of $BmimBF_4$ close to the cationic and anionic regions' boundary, and its nitroxide oxygen forms a hydrogen bond with the acidic imidazolium protons. On the other side, since 4-carboxylate-Tempo samples the nonpolar region made of alkyl chains, its nitroxide oxygen does not form hydrogen bonds. Based on the presented results, one can conclude that Akdogan *et al.*[15] demonstrated the power of EPR spectroscopy in studying the solvation effects in RTILs.

The spin probes Tempo, Tempol, and Cat-1 were used to investigate the micropolarity and microviscosity of the BF_4 and PF_6 based imidazolium RTIL series.[25, 35] Strehmel *et al.*[25] have found that the average rotational correlation time of the three spin probes in those RTILs does not follow the SED theory; instead, they have applied the Gierer–Wirtz theory. According to them, the jumping of the spin probe molecules into the free volume of RTILs is a nonactivated process.

Using EPR spectroscopy, our group has studied the rotational and translational diffusion of spin probe molecules in RTILs.[29-31, 36] Perdeuterated 2,2,6,6-tetramethyl-4-oxopiperidine-1-oxyl (pDTO) has been used to investigate the nanostructural organization of a series of BF_4 based imidazolium RTILs with alkyl chain lengths from two to eight carbon atoms. The SED law well described the rotational correlation time of pDTO in those RTILs.[31] We also studied the translational diffusion of the ^{14}N- and ^{15}N-labeled pDTO at various temperatures in 1-ethyl-3-methylimidazolium bis(trifluoromethylsulfonyl)imide (EmimTFSI) ionic liquid.[29] The temperature dependence of the translation diffusion coefficient of pDTO in EmimTFSI was well explained by the fractional power-law modification of Stokes-Einstein law. In another study,[30] the Heisenberg spin exchange dipole-dipole separation method[36] was used to measure the translational diffusion coefficients of pDTO as a function of temperature in two series of imidazolium RTILs, one based on the BF_4 anion and the other based on the bis(trifluoromethylsulfonyl)imide (TFSI) anion. The obtained translational diffusion coefficients of pDTO were analyzed in terms of the Cohen–Turnbull free volume theory. The translational diffusion of pDTO in all ionic liquids in the measured temperature range was exceptionally well described by the Cohen-Turnbull theory. To the best of our knowledge, there is no analysis of the rotational correlation time of a solute in RTILs done by using the Cohen-Turnbull theory.

Although there are many EPR studies of Cat-1 in RTILs, most of them have been performed at room temperature only. Therefore, we here intend to study the rotational correlation time and hyperfine coupling spacings of the positively charged spin probe Cat-1 in a series of 1-alkyl-3-methylimidazolium BF_4 RTILs with the alkyl chain length from two to eight carbons as a function of temperature. The obtained rotational correlation time results will be analyzed in terms of both the SED and Cohen-Turnbull theories. Also, the rotational diffusion of Cat-1 in RTILs will

be compared to that of pDTO in the same RTILs. This will allow us to investigate the effect of charge on a solute's rotation in ionic liquids.

METHODS

Materials and EPR Spectroscopy

The spin probe Cat-1 (4-trimethylammonium-2,2,6,6-tetramethylpiperidine-1-oxyl iodide, 95% purity) was purchased from Synchem UG & Co. KG and used as received. The RTILs 1-ethyl-3-methylimidazolium tetrafluoroborate ($EmimBF_4$), 1-butyl-3-methylimidazolium tetrafluoroborate ($BmimBF_4$), 1-hexyl-3-methylimidazolium tetrafluoroborate ($HmimBF_4$), and 1-octyl-3-methylimidazolium tetrafluoroborate ($OmimBF_4$) were purchased from IOLITEC. Scheme 1 shows the structures of Cat-1, pDTO, and $EmimBF_4$. Prior to usage, the RTILs had been dried under vacuum for 4 d at 60°C. The solutions of 0.5 mM Cat-1 were prepared by weight in each RTIL. The solutions were drawn into 20 μL capillaries, which were then sealed by an open flame at both ends.

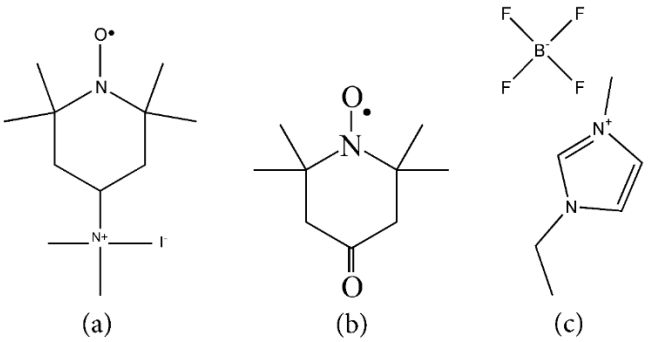

Scheme 1. Structures of (a) Cat-1, (b) pDTO, and (c) $EmimBF_4$.

EPR spectra were measured with a Varian E-109 X-band spectrometer upgraded with a Bruker microwave bridge and a Bruker high-Q cavity. Spectra were acquired using a sweep time of 40 s; sweep width, 50 G; time constant, 16 ms; microwave power, 1 mW; modulation amplitude, 0.44 G. A thermocouple connected to an Omega temperature indicator was placed above and very close to the active region of the EPR cavity to avoid reducing the cavity Q-factor. The sample temperature, controlled by a Bruker variable temperature unit, was held stable within ±0.2 K. The temperature increase interval, 5 K, was the same for all samples, while the temperature range was chosen based on the thermal properties of RTIL.

Analysis of EPR Spectra

EPR spectra, having inhomogeneously broadened lines, were analyzed using the home-written computer program Lowfit, whose fit function is a Lorentzian–Gaussian sum, an excellent approximation of the Voigt shape.[37-38] The shape of the Voigt, which is an excellent approximation of inhomogeneously broadened EPR lines, depends only on the shape parameter $\chi(M_I)$. which is the ratio of the Gaussian component linewidth $\Delta H_{pp}^{G}(M_I)$ to the Lorentzian component linewidth $\Delta H_{pp}^{L}(M_I)$ of the EPR line, where M_I = +1, 0, and −1 represent the low-, middle-, and high-field lines, respectively. Using the procedure described in ref [37], the Lowfit program gives the Lorentzian–Gaussian sum, whose overall line width is $\Delta H_{pp}^{0}(M_I)$, and the percentage of Lorentzian in the sum function, $\eta(M_I)$, which is called the mixing parameter. The Voigt shape parameter is $\chi(M_I)$, can be then calculated from the Lorentzian mixing parameter, $\eta(M_I)$ as detailed in ref [38]. Now, using the Dobryakov-Lebedev relation[39]

$$\left(\frac{\Delta H_{pp}^{G}(M_I)}{\Delta H_{pp}^{0}(M_I)}\right)^2 + \left(\frac{\Delta H_{pp}^{L}(M_I)}{\Delta H_{pp}^{0}(M_I)}\right) = 1 \qquad (1a)$$

or its variation

$$\Delta H_{pp}^{L}(M_I) = \frac{\Delta H_{pp}^{0}(M_I)(-1+\sqrt{1+4\chi(M_I)^2})}{2\chi(M_I)^2} \qquad (1b)$$

one can extract $\Delta H_{pp}^{L}(M_I)$, which can then be used to calculate the rotational correlation times.[38, 40]

According to Akdogan *et al.,*[15] the preferred axis of rotation of Cat-1 is its *x*-axis, which is along the direction of the N–O bond. This rotation is represented by the parallel rotational correlation time $\tau_{R\|}$. The rotation in the plane perpendicular to the *x*-axis is represented by the perpendicular rotational correlation time $\tau_{R\perp}$.[22, 41-42]

Figure 1 shows the experimental EPR spectrum of Cat-1 in $BmimBF_4$ at 308 K together with its fit. The goodness of the fit is illustrated by an almost entirely flat residual, apart from small wiggles. In the case of fast-anisotropic rotational diffusion, the shape of EPR lines contains information not just on the rotation rate but also on the principal (||) axis of rotation of Cat-1. The progressively decreasing EPR line heights, or increasing line broadening from left to right of the spectrum, indicate that the principal (||) axis of rotation of Cat-1 is the *x*-axis, which is along the $NO^{\cdot}$ moiety.[15, 22]

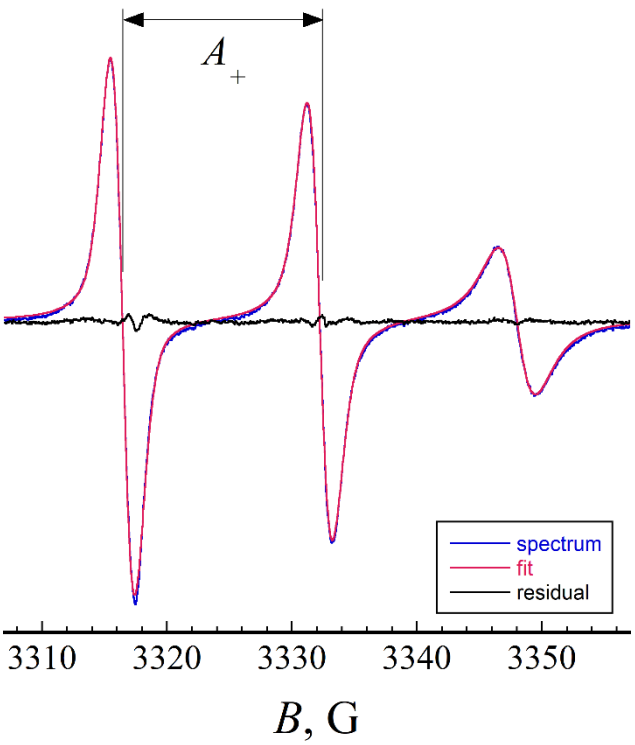

Figure 1. Experimental EPR spectrum (blue line) and fit (red line) of Cat-1 in $BmimBF_4$ at 308 K. A_+ is the difference in the magnetic resonance field position of the center- and low-field lines.

For anisotropic rotational diffusion, which is axially symmetric about the nitroxide *x*-axis, the first step is to calculate the correlation times τ_{20} and τ_{22} (in seconds) from the following equations[22, 41-43]

$$\tau_{20} = \frac{9\sqrt{3}}{8\gamma_e H \Delta A} \frac{5(\delta A)B - 8(\delta g)HC}{\Delta g \delta A - \delta g \Delta A} \qquad (2)$$

$$\tau_{22} = \frac{3\sqrt{3}}{8\gamma_e H \delta A} \frac{8(\Delta g)HC - 5(\Delta A)B}{\Delta g \delta A - \delta g \Delta A}, \qquad (3)$$

where *H, B, C*, *ΔA,* and *δA* are all in gauss. *H* is the magnetic field, and *B* and *C* are parameters that are calculated from the differences in the Lorentzian linewidths[22, 44]

$$B = \frac{1}{2}\left(\Delta H_{pp}^{L}(+1) - \Delta H_{pp}^{L}(-1)\right) \qquad (4)$$

$$C = \frac{1}{2}\left(\Delta H_{pp}^{L}(+1) + \Delta H_{pp}^{L}(-1) - 2\Delta H_{pp}^{L}(0)\right). \qquad (5)$$

In this work, *B* and *C* were calculated from the corresponding line-heights, which are fitted with more precision,[37] and were then corrected for the inhomogeneous broadening of the experimental spectra as described in refs [38] and [22]. The hyperfine coupling constant anisotropies *ΔA* and *δA* are given by

$$\Delta A = A_{xx} - \frac{1}{2}(A_{yy} + A_{zz}) \qquad (6)$$

$$\delta A = \frac{1}{2}(A_{yy} - A_{zz}) \qquad (7)$$

where A_{xx}, A_{yy}, and A_{zz} are the principal values of the hyperfine coupling tensor. Using the hyperfine tensor and *g* tensor principal values of Cat-1 in the RTILs from ref [15], we get

$$\tau_{20} = B_{x0}B + C_{x0}C \qquad (8)$$

$$\tau_{22} = B_{x2}B + C_{x2}C \qquad (9)$$

where the coefficients B_{x0}, C_{x0}, B_{x2}, and C_{x2} for each RTIL are given in Table SI1 (Supplemental Information). Finally, the rotational correlation times $\tau_{R\|}$. $\tau_{R\perp}$ and τ_R are given by[22, 41, 43]

$$\tau_{R\perp} = \tau_{20} \qquad (10)$$

$$\tau_{R||} = \frac{2\tau_{20}}{3\left(\tau_{20}/\tau_{22}\right)-1} \qquad (11)$$

$$\tau_R = \sqrt{\tau_{R||}\tau_{R\perp}} \qquad (12)$$

RESULTS AND DISCUSSION

Temperature Dependence of Rotational Correlation Time and Apparent Activation Energy

The rotational correlation time values τ_R of Cat-1 as a function of temperature in the four ionic liquids are shown in Figure 2. The solid lines through the experimental data are fits to the power-law

$$\tau_R = \tau_{R0}\left(\frac{T}{T_0} - 1\right)^{-\gamma} \qquad (13)$$

where τ_{R0} and γ are constants, and T_0 is the thermodynamic singular temperature. The fit parameters and correlation coefficients (R) of the solid lines in Figure 2 are presented in Table 1. Equation 13 was initially recommended by Speedy and Angell[45] for fitting a variety of liquid water thermodynamic properties in the temperature range 235 to 423 K, which includes both supercooled and normal states. Speedy and Angell found that all analyzed thermodynamic properties can be fitted well to T_0 = 228 K. We have recently used eq 13 to fit the experimentally measured[40] and molecular dynamics (MD) simulated[46] rotational correlation times of four small nitroxide probes in supercooled and normal water and have found that eq 13 fits those data exceptionally well. We have also successfully applied eq 13 to fit the rotational correlation time of pDTO in BF_4 based RTILs and squalane (a viscous alkane), as well as the viscosity of these solvents.[31] One can see in

Figure 2 that τ_R of Cat-1 in the RTILs is described exceptionally well by eq 13, which is also supported by the correlation coefficients, *R,* in Table 1.

Using the mode-coupling theory (MCT),[47-48] we have in detail discussed the reason for using eq 13 with T_0 = 228 K to fit the rotational correlation time of spin probes in RTILs.[31] We believe that it is not necessary to repeat the same discussion here; the interested reader is referred to ref [31]. According to the MCT,[31, 48-49] T_0 could be viewed as a measure of the solvent's spatially heterogeneous dynamics. By assuming the same T_0, we assumed similar heterogeneous dynamics across the variety of solvents we studied.[31, 40] Currently, we do not understand the physical reason for the assumption that heterogeneous dynamics in RTILs is similar to that in supercooled water, so we must stress that using T_0 = 228 K is still empirical. Although empirical, this approach describes the temperature change of the rotational correlation time and viscosity in RTILs extremely well. Comparing the values of γ in Table 1 to the values of γ in Tables 1 and 2 in ref [31], one can notice that they are close to each other for each solvent. This implies that the temperature functional dependences of τ_R of Cat-1 and pDTO in each RTIL are very similar, and in turn, they are similar to the temperature functional dependence of η.

Table 1. Power Law $\tau_R = \tau_{R0}(T/(228\text{ K}) - 1)^{-\gamma}$ Parameters for τ_R of Cat-1 in Ionic Liquids and Correlation Coefficient, *R*.

	τ_{R0}, ns	γ	R
$EmimBF_4$	0.0151±0.0005	2.82±0.03	0.9995
$BmimBF_4$	0.0120±0.0002	3.79±0.02	0.9999
$HmimBF_4$	0.0123±0.0002	4.23±0.02	0.9999
$OmimBF_4$	0.0125±0.0001	4.53±0.01	0.9999

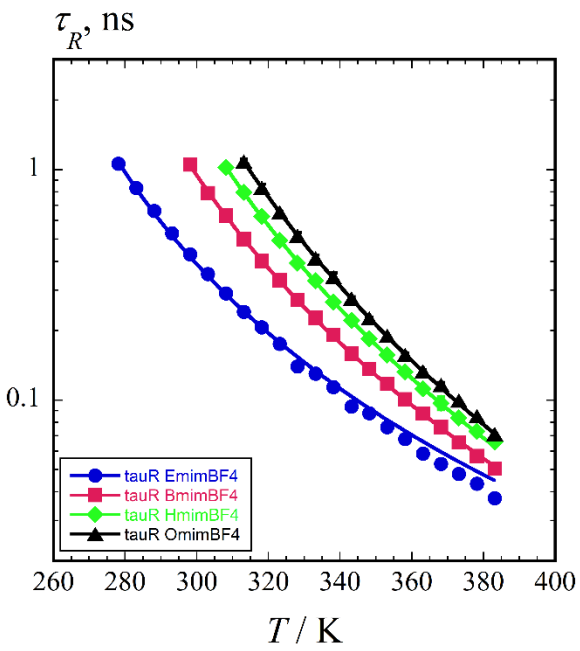

Figure 2. Rotational correlation time τ_R of Cat-1 as a function of temperature in $EmimBF_4$ (●), $BmimBF_4$ (■), $HmimBF_4$ (◆), and $OmimBF_4$ (▲). The solid lines are fits to $\tau_R = \tau_{R0}(T/(228\ \mathrm{K}) - 1)^{-\gamma}$, and the fitting parameters τ_{R0} and γ are given in Table 1.

The temperature effect on the rotational correlation time is often described by the Arrhenius equation

$$\tau_R = \tau_{R0} \exp(-\frac{E_A}{RT}) \qquad (14)$$

where E_A is a constant called the activation energy, R is the universal gas constant, and τ_{R0} is τ_R at $T = \infty$. E_A is the slope of the line $(d(\ln(\tau_r))/d(1/RT))$ plotted in the ln τ_R versus $1/T$ graph, so it represents the sensitivity of τ_R to temperature. In many cases when experimental data, especially transport properties in supercooled liquids, are plotted in the ln τ_R versus $1/T$ graph,[31, 49-51] the data cannot be fitted to a line, which indicates that E_A is temperature-dependent, or that the studied property exhibits non-Arrhenius behavior. In this case, calculating the slope of the curve at a given temperature gives the temperature-dependent apparent activation energy $E_{app}(T)$[52] as

$$E_{app}(T) = R\frac{dln(\tau_r(T))}{d(\frac{1}{T})} = -RT^2\frac{dln(\tau_r(T))}{d(T)} = \frac{\gamma RT^2}{T-T_0} \qquad (15)$$

Figure 3 shows the apparent activation energies for τ_R. The apparent activation energy increases with increasing alkyl chain length, and for each solvent, it increases with decreasing temperature. The value of E_A is directly proportional to the value of the exponent γ when T_0 = constant for different solvents. Comparing the values of E_{app} for Cat-1 and pDTO, or their γ equivalents, $EmimBF_4$ appears different from the other three RTILs. For $EmimBF_4$, the value of γ for Cat-1 is 2.82 (Table 1) and is less than γ(pDTO) = 2.965,[31] which means that E_{app}(Cat-1) < E_{app}(pDTO). On the other hand, the γ values 3.79 ($BmimBF_4$), 4.23 ($HmimBF_4$), and 4.53 ($OmimBF_4$) for Cat-1 (Table 1) are greater than the γ values 3.564 ($BmimBF_4$), 4.08 ($HmimBF_4$), and 4.33 ($OmimBF_4$) for pDTO.[31] Therefore, the apparent activation energies for the rotation of Cat-1 in $BmimBF_4$, $HmimBF_4$, and $OmimBF_4$ are greater than those for the rotation of pDTO in the same RTILs.

These results can be explained in light of the nanostructural organization of the studied RTILs. Generally, RTILs form a liquid nanostructure with coexisting polar and nonpolar nanodomains.[53-54] In $EmimBF_4$, the polar domain consists of a continuous three-dimensional ionic channel network, interspersed with small globular nonpolar domains. These two domains look homogeneously distributed (Figure 11 in ref [53]). Since the Emim cation is too small and the alkyl chain is too short, these structures cannot be regarded as nanodomains. As the alkyl chain grows, the nonpolar domains increase and interconnect, forming the second three-dimensional network. For the alkyl chains greater than C_4, the two three-dimensional networks form a bi-continuous spongelike nanostructure.[53-54] Therefore, in $EmimBF_4$, which consists of homogeneously distributed polar and nonpolar domains, the electrostatic interaction between the positive charge of Cat-1 and BF_4^- is not as strong as in the RTILs with longer alkyl chains, whereas in the case of the spongelike nanostructure, Cat-1 might be positioned deeper into the polar domain, which

increases its electrostatic interaction and, in turn, the apparent activation energy. The biggest change in E_{app} between $EmimBF_4$ and $BmimBF_4$ observed in Figure 3 probably indicates a change in nanostructure morphology when the alkyl side chain is four carbons long.

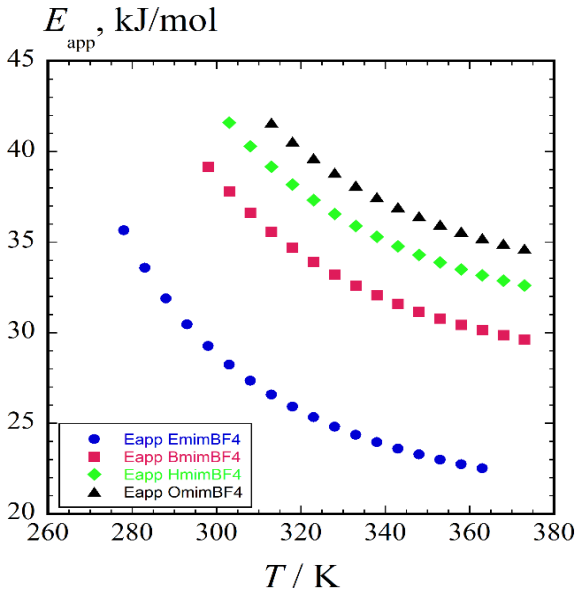

Figure 3. Apparent activation energy for τ_R of Cat-1 versus T in $EmimBF_4$ (●), $BmimBF_4$ (■), $HmimBF_4$ (◆), and $OmimBF_4$ (▲).

Stoesser *et al*.[27] found that the average rotational time of Cat-1 in a series of ionic liquids based on substituted imidazolium cations and tetrafluoroborate anion measured at 20 ºC is proportional to the alkyl chain length. In the same way, in Figure 4, we observe that our τ_R data versus the alkyl chain length can be fitted to straight lines with positive slopes at each temperature. The slope of the lines decreases with increasing temperature. This suggests that the microenvironment sensed by the probe at higher temperatures is becoming more alike.

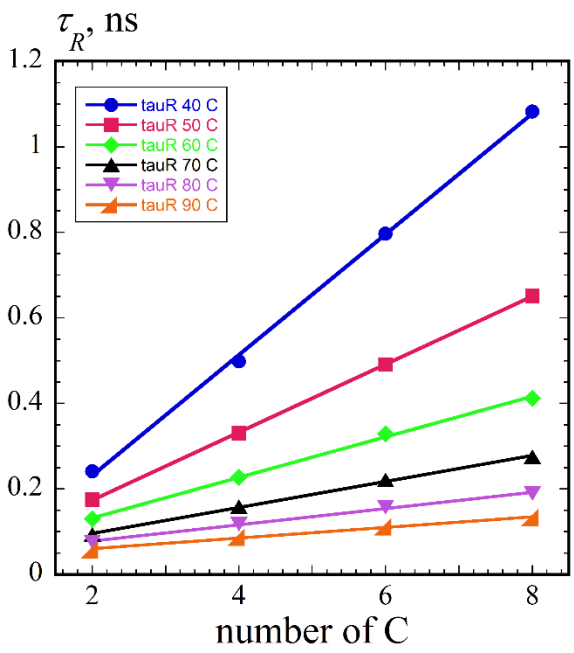

Figure 4. τ_R as a function of the length of the alkyl chain at 40 ºC (●), 50 ºC (■), 60 ºC (◆), 70 ºC (▲), 80 ºC (▼), and 90 ºC (◢). The solid lines are linear fits to the data; all Rs are greater than 0.998.

Rotational Anisotropy

The parallel and perpendicular rotational correlation times of Cat-1 in RTILs are calculated to estimate τ_R, and they are plotted in Figures 5 a and b. Again, these data can be fitted quite well to eq 13. The fits are represented by the solid lines in Figures 5 a and b, and the fitting parameters are given in Table 2. Although the values of γ for $\tau_{R\|}$ and $\tau_{R\perp}$ of Cat-1 in $EmimBF_4$ are close, they start diverging as the length of the alkyl chain increases. The values of γ for $\tau_{R\|}$ in the case of $BmimBF_4$, $HmimBF_4$, and $OmimBF_4$ are greater than the values of γ for $\tau_{R\perp}$. Additionally, the values of $\tau_{R0\perp}$ are greater than those of $\tau_{R0\|}$ by a factor of 2.6 for $EmimBF_4$ to a factor of 6 for $OmimBF_4$ (compare the 2nd and 5th columns in Table 2).

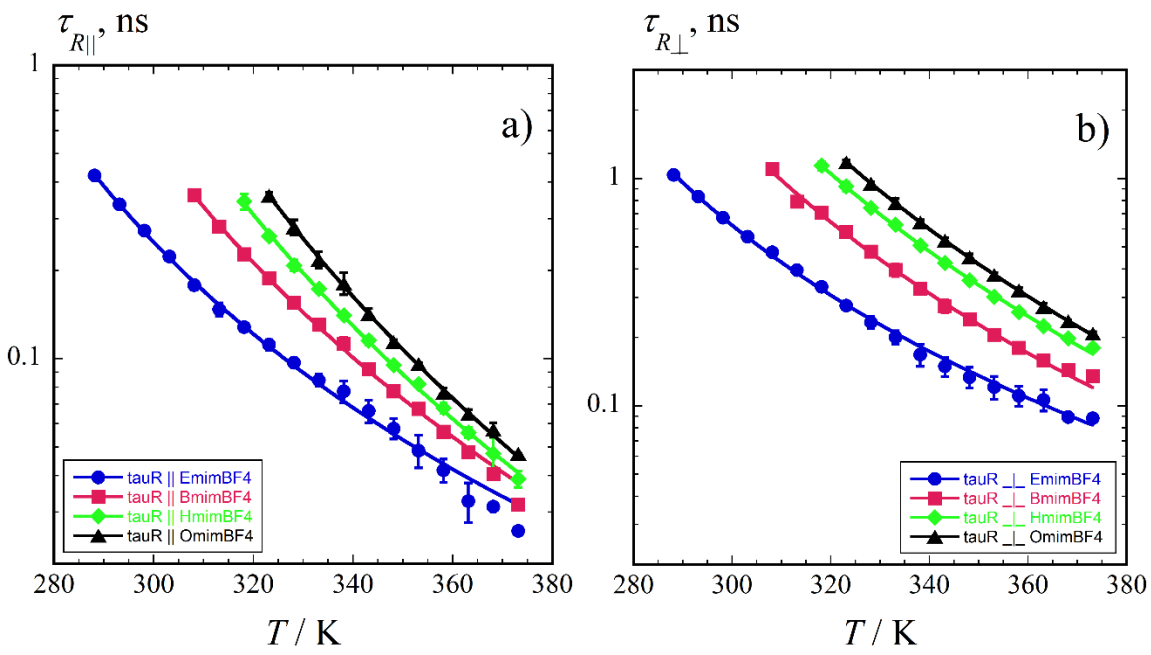

Figure 5. Rotational correlation times $\tau_{R||}$ (a) and $\tau_{R\perp}$ (b) of Cat-1 as a function of temperature in $EmimBF_4$ (●), $BmimBF_4$ (■), $HmimBF_4$ (◆), and $OmimBF_4$ (▲). The solid lines are fits to $\tau_R = \tau_{R0}(T/(228\ K) - 1)^{-\gamma}$, and the fitting parameters $\tau_{R0||}$, $\tau_{R0\perp}$, and γ are given in Table 2.

Table 2. Power Law $\tau_R = \tau_{R0}(T/(228\ K) - 1)^{-\gamma}$ Parameters for $\tau_{R||}$ and $\tau_{R\perp}$ of Cat-1 in Ionic Liquids and their Correlation Coefficients, *R*.

	$\tau_{R0||}$, ns	γ	R	$\tau_{R0\perp}$, ns	γ	R
$EmimBF_4$	0.0084±0.0003	2.94±0.03	0.999	0.0223±0.0007	2.89±0.03	0.999
$BmimBF_4$	0.0068±0.0002	3.79±0.04	0.999	0.0228±0.0020	3.68±0.09	0.997
$HmimBF_4$	0.0055±0.0002	4.44±0.05	0.999	0.0278±0.0006	4.00±0.03	0.999
$OmimBF_4$	0.0052±0.0003	4.85±0.04	0.999	0.0314±0.0003	4.15±0.01	0.999

The details of the axially anisotropic rotational diffusion of Cat-1 can be further revealed by plotting $\tau_{R\perp}$ versus $\tau_{R||}$, Figure 6a. It appears that the data can be satisfactorily fitted to straight lines. The line's slope is usually called the rotational anisotropy *N* ($\tau_{R\perp}/\tau_{R||}$). The values of *N* extracted from Figure 6a are given in Table 3. The rotational anisotropy of Cat-1 is the lowest in $EmimBF_4$, and it increases with increasing alkyl chain length up to $HmimBF_4$ and then remains the same in $OmimBF_4$ (Figure 6a). The rotational diffusion anisotropy of Cat-1 in $BmimBF_4$ of 2.94 observed in this work is similar to those observed in ref [15], which were 3.1 and 4.4. The two

values are presented because the authors assumed that the perpendicular rotation was also anisotropic, that is, $\tau_{Ryy} \neq \tau_{Rzz}$.

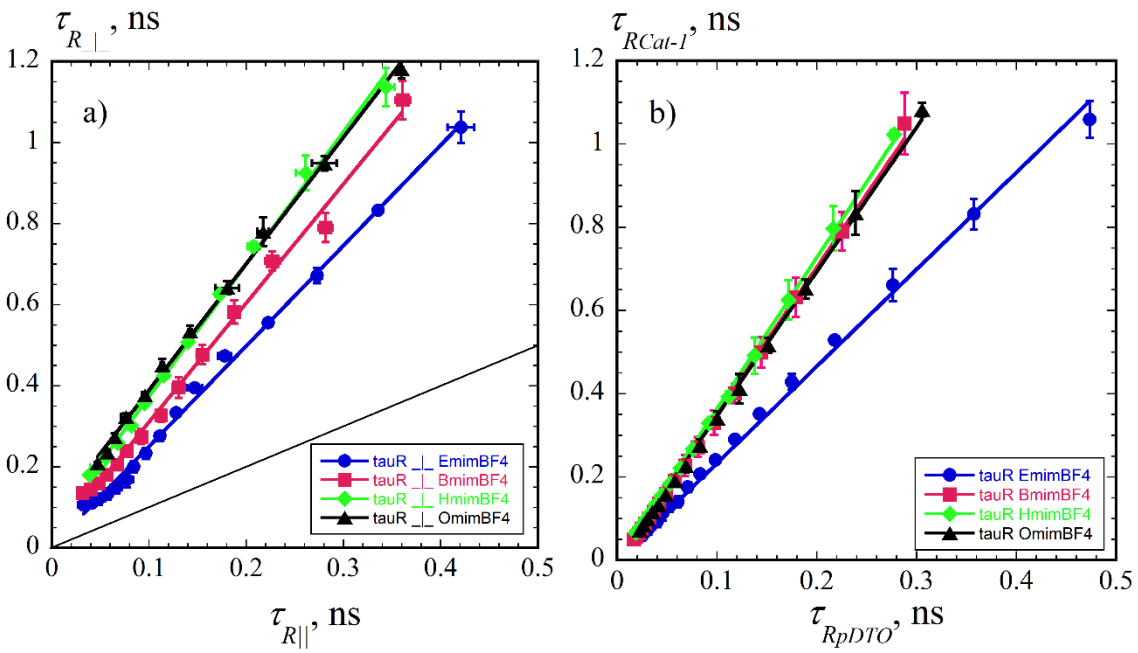

Figure 6. (a) $\tau_{R\perp}$ versus $\tau_{R\parallel}$ for the rotational diffusion of Cat-1 in $EmimBF_4$ (●), $BmimBF_4$ (■), $HmimBF_4$ (◆), and $OmimBF_4$ (▲). The solid lines through the data points are linear fits whose slopes, N, are given in Table 3, while the thin black line has a slope of unity. (b) τ_R of Cat-1 versus τ_R of pDTO in $EmimBF_4$ (●), $BmimBF_4$ (■), $HmimBF_4$ (◆), and $OmimBF_4$ (▲). The solid lines are linear fits whose slopes are presented in Table 3.

Table 3. Rotational Anisotropy N of Cat-1 and the Ratio of the Rotational Correlation Times of Cat-1 and pDTO with their Correlation Coefficients, *R*.

	N	R	$\tau_{R\ Cat\text{-}1}/\tau_{R\ pDTO}$	R
$EmimBF_4$	2.48±0.04	0.998	2.33±0.02	0.998
$BmimBF_4$	2.94±0.06	0.997	3.52±0.03	0.999
$HmimBF_4$	3.26±0.05	0.999	3.63±0.02	0.999
$OmimBF_4$	3.12±0.05	0.999	3.46±0.02	0.999

The fact that $\tau_{R\perp}$ is greater than $\tau_{R\parallel}$ with the values of *N* between 2.48 and 3.12 could be partly explained by the prolate shape of the Cat-1 probe along the ammonium group's direction. Additional reasons behind the faster rotation about the molecular *x*-axis could be (i) the electrostatic interaction of the ammonium group ($-N(CH_3)_3^+$) at the 4-position of the spin probe

with the BF_4^- anion in RTIL and (ii) the hydrogen bonding between the nitroxide group of Cat-1 and the acidic imidazolium protons.[15] Such reasoning is in accordance with the measured rotational anisotropy of PADS (potassium peroxylamine disulfonate) probe in RTILs.[55] This probe contains two negatively charged sulfonyl groups and exhibits more substantial anisotropy in RTILs (N = 3-5) than Cat-1. The N values of PADS in RTILs were found to be larger than the value N = 2.4 of PADS in organic solvent *N*-methylimidazole and the theoretical value N = 1.4 calculated from the prolate shape of PADS. These findings suggest that rotational anisotropy of PADS in RTILs is strongly influenced by the Coulombic interaction between the sulfonyl groups and the RTIL cations.[55]

The change in N as a function of C (Figure 6a and Table 3), very possibly, reflects the transition between the homogeneously globular structure and the sponge-like structure, Figure 11 in ref [53], which happens at C_4, that is, in $BmimBF_4$.

The rotational correlation times of Cat-1 and pDTO are compared in Figure 6b. The ratio $\tau_{RCat\text{-}1}/\tau_{RpDTO}$ is temperature-independent, and the slopes of the fits are given in Table 3. In $EmimBF_4$, the rotation of Cat-1 is 2.33 times slower than the rotation of pDTO, while in the other three RTILs, it is about the same, and it is 3.5 times slower. The main reason for the slower rotation of Cat-1 is the ammonium group's existence and its charge. The sudden jump in $\tau_{RCat\text{-}1}/\tau_{RpDTO}$ from $EmimBF_4$ to $BmimBF_4$ is likely caused by the transition between the two ionic liquid morphologies, as in the case of activation energy (Figure 3).

Rotational Correlation Time in Terms of the SED Theory

The viscosity dependence of the rotational diffusion of a probe particle of volume V is

usually given by the SED equation

$$\tau_R = f\frac{V\eta}{kT} \qquad (16)$$

where η is the shear viscosity of the surrounding liquid, k is the Boltzmann constant, and f is the slip coefficient. This equation is derived from the hydrodynamic theory for the rotation of a Brownian particle in a homogeneous liquid consisting of molecules that are much smaller than the Brownian particle. In this case, the solvent molecules at the particle's surface have zero tangential velocity, which implies that they rotate together with the particle. Under these conditions, f is equal to unity, and it represents the so-called stick or no-slip boundary condition. When the particle and liquid molecules' sizes are comparable, the slip coefficient is less than unity. In this case, the slip coefficient f becomes an indicator of interactions between the particle and its surroundings.

Commonly, the volume of probe V is given by its van der Waals volume. The van der Waals volume is the probe's minimal impenetrable volume that does not change with temperature.[56-57] The rotational correlation time of Cat-1 in RTILs as a function of η/T is shown in Figure 7. The solid lines are linear fits (without intercept), whose slopes and correlation coefficients, R, which are all equal to 0.999, are given in Table 4. Since the values of τ_R in Figure 7 are much shorter than the ones expected from eq 16 for a spherical van der Waals particle with stick boundary condition, f can be treated as the ratio of an effective hydrodynamic volume to the van der Waals volume of the probe, that is, $V_H/V_{vdW} = (r_H/r_{vdW})^3$.

Following the procedure from ref [58], one finds that the van der Waals volume of Cat-1 without iodide is 229.61 Å^3, while the van der Waals volume of pDTO is 177.46 Å^3. The corresponding van der Waals radii are 3.80 Å for Cat-1 and 3.48 Å for pDTO. The van der Waals

volumes of the RTILs are 192 Å^3 for $EmimBF_4$, 226.5 Å^3 for $BmimBF_4$, 261 Å^3 for $HmimBF_4$, and 296 Å^3 for $OmimBF_4$. The values of the effective Cat-1 radii, their ratios with respect to the van der Waals radius, and their slip coefficients in RTILs are all presented in Table 4. The effective hydrodynamic radius of Cat-1 in all four RTILs is about half of the van der Waals value, and it decreases from 59 to 52% of r_{vdW} as the alkyl chain's length increases. These low effective radius values give very low slip coefficients ranging from 0.21 to 0.14, which indicate that, although charged, Cat-1 rotates quite freely in the studied RTILs. The effective hydrodynamic radii of pDTO in the same RTILs are even lower, decreasing from 52 to 37% of r_{vdW} with increasing length of the hydrocarbon chain (Table 4). These values give lower slip coefficients ranging from 0.14 to 0.051.

The higher values of the hydrodynamic radius for Cat-1 presented above can be explained by the charge of Cat-1 and its bigger size due to the ammonium group. The decrease of the effective hydrodynamic radius with increasing alkyl chain length in both cases is due to the increasing nonpolar domains. The fractional change of $r_{HCat\text{-}1}$ from $EmimBF_4$ to $OmimBF_4$, which is half of the fractional change of r_{HpDTO} in the same RTILs, supports the idea that Cat-1 is mostly located in the polar region[15] and, therefore, is less affected by the growth of the nonpolar regions.

Table 4. SED Slope, $\tau_R/(\eta/T)$, Correlation Coefficient R, Effective Hydrodynamic Radius of Cat-1 in Ionic Liquids. The Ratios of the Effective Hydrodynamic Radius to the van der Waals Radius of Cat-1 and pDTO in Ionic Liquids and the Corresponding Slip Coefficients in Parenthesis.

	SED slope, ns·K·m^3/mPas	R	r_H, Å	$\frac{r_{HCat-1}}{r_{vdW}}$ (f)	$\frac{r_{HpDTO}}{r_{vdW}}$ (f)
$EmimBF_4$	3.50±0.01	0.999	2.26	0.59 (0.21)	0.52 (0.14)
$BmimBF_4$	2.97±0.01	0.999	2.14	0.56 (0.19)	0.40 (0.064)
$HmimBF_4$	2.59±0.02	0.999	2.03	0.53 (0.15)	0.38 (0.055)
$OmimBF_4$	2.38±0.01	0.999	1.99	0.52 (0.14)	0.37 (0.051)

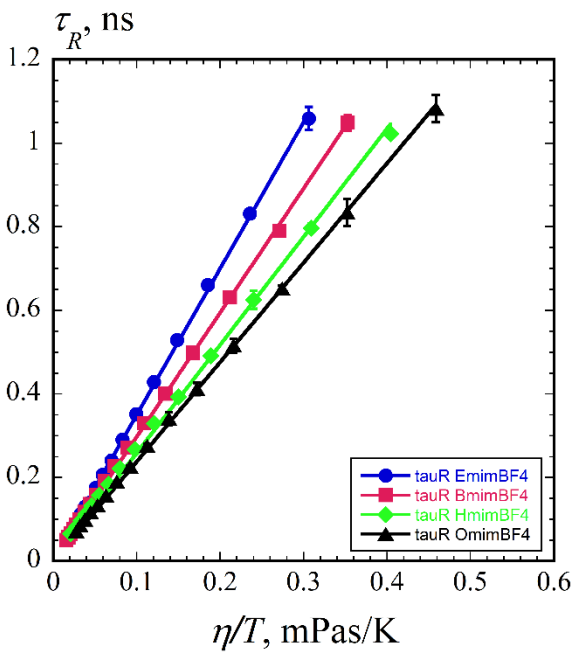

Figure 7 Rotational correlation time τ_R of Cat-1 versus η/T in $EmimBF_4$ (●), $BmimBF_4$ (■), $HmimBF_4$ (◆), and $OmimBF_4$ (▲). The solid lines are linear fits (without intercept), whose slope parameters are given in Table 4.

Rotational Correlation Time in Terms of Free Volume

Transport properties of ionic liquids (self-diffusion, tracer diffusion, viscosity, and conductivity) can be analyzed in terms of free volume.[30, 57, 59] Seven decades ago, Frenkel published one of the first models of free volume in liquids.[60] Next, Doolittle was able to precisely and accurately measure alkane densities,[61] which allowed him to estimate the total compressible free volume in alkanes. Using those measured values of free volume, Doolittle found empirically that the alkane's viscosity can be described by an exponential function of the fractional free volume. [61] Finally, using simple theoretical arguments, Cohen and Turnbull were able to describe translational diffusion in terms of free volume. [62-63]

The free volume analysis is based on the idea that in a liquid, at the molecular level, there is an empty space between the liquid molecules. The geometry of this empty space is continuously

changing due to thermal fluctuations. The empty space is commonly called the free volume. The diffusion of either a solvent or a solute molecule can be explained as jumping without any energy expenditure between these successive holes (cages) appearing in the molecule's neighborhood. Intuitively, one can imagine either a solvent or a solute molecule rotating in each of these cages before moving on to the next cage, which means that the molecule's rotation may be affected by the properties of the cage. As far as we know, no one so far has tried to describe the rotational diffusion of a tracer molecule in ionic liquids in terms of free volume. For the first time, we attempt to describe the rotational diffusion of Cat-1 and pDTO as a function of free volume.

Since τ_R follows the SED equation (eq 16), we can use eq 5 from ref [30], which describes the viscosity as a function of free volume, to find the free volume dependence of τ_R as

$$\tau_R = \frac{\tau_{R0}}{\sqrt{T}} \exp\left(\frac{\gamma V^*}{V_f}\right) \qquad (17)$$

where γ is a constant of order unity, γV^* is the critical (minimum) free volume for the rotation of a solute or solvent molecule to occur, and V_f is the free volume per solvent molecule. Equation 17 is the Cohen-Turnbull equation[62-63] for the rotational diffusion of a tracer molecule.

Quite often, it is not easy to obtain an experimental estimate V_f for a liquid, but recently the free volumes of several imidazolium ionic liquids were characterized and analyzed by positron annihilation lifetime spectroscopy.[57, 64-66] We used those free volumes to analyze the translational diffusion of pDTO in two methylimidazolium RTIL series, one based on the BF_4 anion, as in this work, and another one on the bis(trifluoromethane)sulfonimide (Tf_2N, TFSI) anion. The procedure to calculate the free volume from the density of an RTIL is described in detail in ref [30].

Figure 8a,b shows $\tau_R T^{1/2}$ of Cat-1 and pDTO as a function of V_f, respectively. The solid lines are fits to eq 17, whose parameters are tabulated in Table 5. The correlation coefficients, *R*,

in Table 5 and Figures 8a,b indicate excellent fits. As expected, due to the hydrodynamic behavior of the rotation of Cat-1 and pDTO (eq 16), the critical volumes for the rotation of Cat-1 and pDTO (Table 5) are very close to the critical volumes for the viscosity (Table 4 in ref [30]). This suggests that the pre-exponential factor contains the physics of the solvent's effect on the rotation of the solute. Since the pre-exponential factor's meaning is now unknown, we believe it might be an interesting theoretical research point.

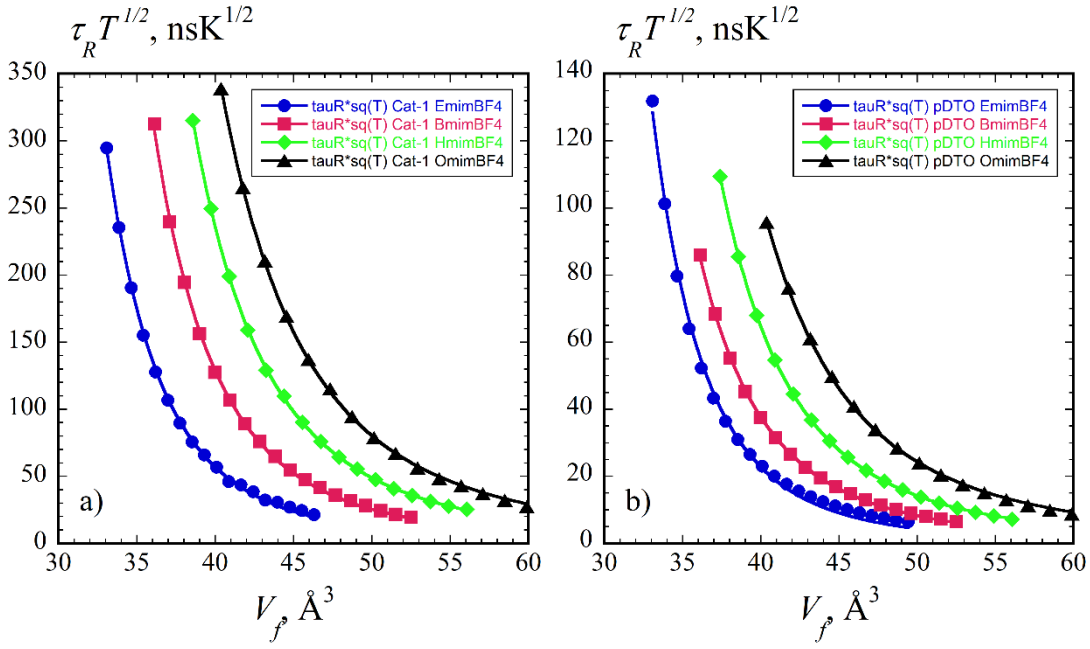

Figure 8. Rotational correlation time τ_R times the square root of temperature of (a) Cat-1 and (b) pDTO as a function of V_f in $EmimBF_4$ (●), $BmimBF_4$ (■), $HmimBF_4$ (◆), and $OmimBF_4$ (▲). The lines are fits to the Cohen-Turnbull equation, eq 17, whose parameters are presented in Table 5.

Table 5. Fit Parameters for the Rotational Correlation Time of Cat-1 and pDTO in RTILs, according to the Cohen-Turnbull Equation, eq 17, and Correlation Coefficients, *R*.

	τ_{R0}, ps·K$^{1/2}$ (Cat-1)	γV^*, Å^3 (Cat-1)	R	τ_{R0}, ps·K$^{1/2}$ (pDTO)	γV^*, Å^3 (pDTO)	R
$EmimBF_4$	22.3±1.3	314±2	0.9998	5.7±0.6	331±3	0.9988
$BmimBF_4$	38.6±2.3	324±2	0.9997	18.9±1.0	304±1	0.9999
$HmimBF_4$	89.6±2.2	315±1	0.9999	32.8±0.1	303±1	0.9999
$OmimBF_4$	186.9±5.7	303±1	0.9999	75.2±1.7	289±1	0.9999

Using ^{17}O NMR T_1 measurements, Yasaka and Kimura[19] have studied the rotation of CO in a series of methylimidazolium-TFSI RTILs. They found that the rotational correlation time τ_{2R} of CO can be fitted well to the fractional SED law

$$\tau_{2R} = \tau_{2R}^0 \left(\frac{\eta}{T}\right)^P \qquad (18)$$

where τ_{2R}^0 and P are solvent-dependent constants. Using the parameters from Table 2 in ref [19], we have plotted the values of τ_{2R} of CO in RTILs as a function of V_f and fitted them to eq 17 (Figure 9). Again, the fits are excellent. The critical volumes for the rotation of CO are smaller than the critical volumes for the viscosity of the corresponding TFSI RTILs (compare the third and fifth columns in Table 6). The ratio of the critical volumes for the rotation of CO and viscosity (sixth column in Table 6) matches the exponent P in eq 18 (seventh column in Table 6).

According to the presented data, a solute's rotational correlation time can be described in terms of the free volume model (eq 17). The critical volumes for the rotation of Cat-1 and pDTO appear close to each other and close to the critical volumes of viscosity. Hence, we believe that if the rotation follows hydrodynamic behavior ($\propto \frac{\eta}{T}$), the critical volumes for rotation and viscosity are similar. If the rotation of a solute deviates from the hydrodynamic theory, as in the case of the CO rotation,[19] the critical volumes are very different, and the critical volume for rotation is less than the one for viscosity. The ratios of the two critical volumes are very close to the fractional

powers of η/T (Table 6). In terms of free volume, one can say that the rotating solute needs a lower critical volume for rotation than is necessary for the viscous flow of the solvent and therefore behaves non-hydrodynamically.

Table 6. Fit Parameters for the Rotational Correlation Time of CO in RTILs, according to the Cohen-Turnbull Equation (eq 17); second – third Columns), and Correlation Coefficent *R*. The Critical Volume for Viscous Flow, $\gamma V^*(\eta)$, the Ratio of Critical Volumes, $\gamma V^*/\gamma V^*(\eta)$, and the Fractional SED Exponent, *P*.[a]

	τ_{R0}, ps $K^{1/2}$ (CO)	γV^*, Å^3 (CO)	R	$\gamma V^*(\eta)$, Å^3	$\gamma V^*/\gamma V^*(\eta)$	*P*
EmimTFSI	0.153 ± 0.010	287 ± 3	0.999	388±4	0.74	0.77
BmimTFSI	0.160 ± 0.009	299 ± 3	0.999	426±4	0.70	0.73
OmimTFSI	0.315 ± 0.005	270 ± 1	0.999	407±2	0.66	0.69

a) The data were taken from ref [19].

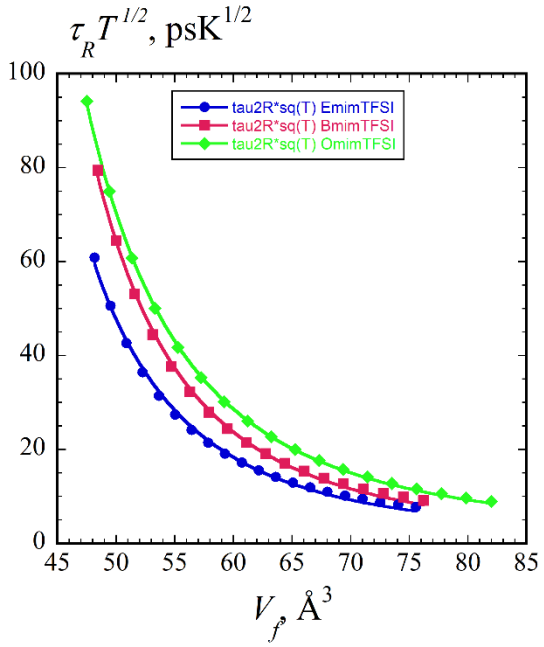

Figure 9. Rotational correlation time τ_{2R} times the square root of temperature of CO as a function of V_f in EmimTFSI (●), BmimTFSI (■), and OmimTFSI (◆). The lines are fits to the Cohen-Turnbull equation (eq 17), whose parameters are presented in Table 6; second – third columns.

Hyperfine Coupling Constant

The hyperfine coupling constant is sensitive to solvent polarity and hydrogen bonding.[22] The greater the polarity of the solvent, the greater the hyperfine coupling constant. Here, instead of using the hyperfine coupling constant A_0, which is one-half the difference in the magnetic resonance field of the high- and low-field EPR lines, neglecting second-order dynamic shifts, we use the hyperfine coupling spacings A_+ (Figure 1), which is the difference in the magnetic resonance fields of the center- and low-field lines. One reason is to minimize the second-order dynamics shifts, and the other is that A_+ is measured with more precision, especially when the EPR lines are broad.[67] Figure 10 shows A_+ of Cat-1 in RTILs versus temperature. As expected, the values of A_+ decrease as the alkyl chain length increases from C_2 to C_8, indicating a reduction in micropolarity with increasing chain length. Another prominent feature of the data is a decrease with increasing temperature.

It is well known that in the fast-motional regime, the nitrogen hyperfine coupling constant is linearly dependent on temperature.[31-32, 68-69] The negative slopes of A_+ observed for Cat-1 in Figure 10 is the same as the decrease in A_{abs} with temperature for TEMPO and TEMPOL in $BmimBF_4$ observed by Mladenova et al. (Figure 4a of ref [32]). On the other hand, it is opposite to the increase in A_{abs} observed for pDTO in C_nmimBF_4, where n = 2, 4, 6, and 8.[31] According to Bullock and Howard[70] and Mladenova *et al.*[32], the temperature dependence of A indicates the out-of-plane or umbrella vibrations of the equilibrium $C_2N\text{-}O^{\cdot}$ center structure in the radical, which can be either planar or pyramidal. In the case of Tempo and Tempol, whose angles between the $N\text{-}O^{\cdot}$ bond and the C_2N plane in solid are 19.4 and 15.8°, respectively, the temperature coefficients of A observed in RTILs are negative,[32] indicating non-planarity. The positive temperature

coefficients of A observed for pDTO in RTILs indicate planarity, that is, the same zero angle between the N-O˙ bond and the C_2N plane as observed in solid.[71] The negative temperature coefficients of A_+ for Cat-1in RTILs (Figure 10 and Table 7) strongly suggest that the configuration of the C_2N-O˙ center in those solvents is non-planar, pyramidal having symmetric double minimum potential with a significant inversion barrier[70] as in the case of Tempo and Tempol. It is possible that the angle between the N-O˙ bond and the C_2N plane in Cat-1 is somewhere between 10 and 20º. The magnitude of dA_+/dT decreases from $OmimBF_4$ to $EmimBF_4$, Table 7, which means that the umbrella vibrations' energy quanta are shifted to larger energies in the same direction.[32]

The hyperfine coupling temperature coefficient dA_+/dT of Cat-1 in RTILs as a function of relative permittivity ε_r is shown in Figure 11 and Table 7. The relative permittivity values from ref [72] are calculated values and are very close to the experimental values, which are presented in the Supplemental Information. In Figure 11, one can see that the temperature coefficients are directly proportional to the relative permittivity. Ottaviani *et al.*[69] studied the physicochemical properties of four small nitroxide probes, one of which was Cat-1, in polar hydrogen bond acceptor solvents and hydroxylic solvents as a function of temperature. They found that the values of A_N of Cat-1 in all studied solvents decrease with increasing temperature, the same way as it was observed in this work. Figure 11 shows the hyperfine coupling temperature coefficients as a function of ε_r in the RTLS and alcohols (methanol to butanol – data taken from ref [69]). One can observe that dA_+/dT behaves similarly in both series; the slopes become less negative with increasing ε_r.

Ottaviani *et al.* [69] also explained the hyperfine coupling temperature slopes change in terms of changing hydrogen bond donor (HBD) capacity. Padró and Reta[73] obtained the HBD acidity parameter α for a series of 1-alkyl-3-methylimidazolium hexafluorophosphate (n = 4, 6, and 8).

The HBD capacity of the imidazolium-based RTILs comes from the hydrogen atom attached to C_2 of the imidazolium ring, which forms a hydrogen bond with the NO˙ moiety of Cat-1. α values equal to 0.64 ± 0.02 for $BmimPF_6$, 0.62 ± 0.02 for $HmimPF_6$, and 0.58 ± 0.02 for $OmimPF_6$ indicate that the HBD capacity decreases with the alkyl chain length. We have not found the values of α for the imidazolium BF_4 RTILs except for $OmimBF_4$, which is 0.60 ± 0.02.[73] Nevertheless, in the case of imidazolium BF_4 RTILs, one would expect the same behavior. In other words, the strength of hydrogen bonding between the C_2 hydrogen and the Cat-1 oxygen decreases with increasing alkyl chain length. Therefore, one can conclude that the hyperfine coupling temperature slope becomes more negative with decreasing α or increasing chain length, as in alcohols.

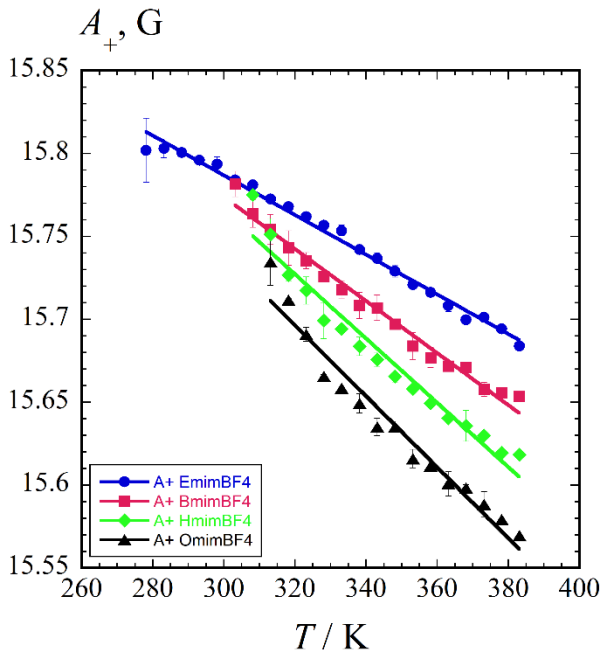

Figure 10. Hyperfine coupling spacings A_+ of Cat-1 versus T in $EmimBF_4$ (●), $BmimBF_4$ (■), $HmimBF_4$ (◆), and $OmimBF_4$ (▲). The straight solid lines are linear fits, whose coefficients are given in Table 7.

Table 7. Temperature Coefficients $dA_{+(N)}/dT$ of Cat-1 in RTILs and Alcohols.

	dA_{+}/dT 10^{-3} (G/K)	ε_r
$EmimBF_4$	-1.19 ± 0.03	14.8[a]
$BmimBF_4$	-1.57 ± 0.05	12.9[a]
$HmimBF_4$	-1.94 ± 0.10	11.3[a]
$OmimBF_4$	-2.14 ± 0.12	7.5[a]
Methanol	-1.3[b]	32.1[b]
Ethanol	-1.7[b]	23.8[b]
1-Propanol	-1.9[b]	20.0[b]
2-Propanol	-2.0[b]	19.5[b]
1-Butanol	-2.3[b]	17.3[b]

[a] Data taken from ref [72], [b] Data taken from ref [69].

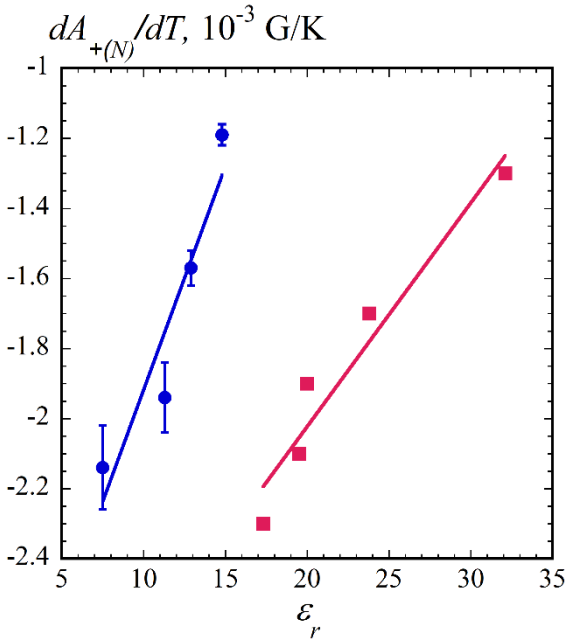

Figure 11. Temperature coefficients dA_{+}/dT of Cat-1 in RTILs (●) and alcohols (■). The alcohol data were taken from ref [69]. Solid lines are linear fits.

CONCLUSIONS

Using nonlinear least-squares fitting of the EPR spectra, the rotational correlation time and hyperfine coupling splitting of Cat-1 in RTILs have been obtained with high precision. The mean rotational correlation time, as well as the parallel and perpendicular correlation times as a function of temperature, have been exceptionally well described by a power-law relationship with a singular temperature. The parallel rotation of Cat-1 along its x-axis in RTILs is 2.5 to about 3 times faster than its perpendicular rotation in the y-z plane. Cat-1 is likely located in the polar region of each RTIL close to the cationic and anionic regions' interface, as suggested by Akdogan *et al.*[15] The SED equation fully describes the mean rotational correlation times of Cat-1 in RTILs. At the same time, the calculated apparent activation energy indicates non-Arrhenius behavior. The uneven spacing of the apparent activation energy, the rotational anisotropy N, and $\tau_{R\ Cat\text{-}1}/\tau_{R\ pDTO}$ imply that the RTILs whose alkyl chains have more than four carbons have a structure different from that of $EmimBF_4$, which is well established by MD simulations. Also, the hyperfine coupling temperature slope of Cat-1 in RTILs increases with decreasing HBD capacity of the hydrogen atom attached to C_2 of the imidazolium ring.

The rotational correlation time of Cat-1 in RTILs can be described as a function of V_f using the Cohen-Turnbull equation. The critical volumes for the rotation of Cat-1 are close to the viscosity's critical volumes of the RTILs, indicating the hydrodynamic nature of the rotation. The critical volumes for the rotation of CO in RTILs, taken from the literature, are less than those for the viscous flow of the RTILs. The ratio of the critical volumes for τ_R and η is similar to the SED fractional exponent in eq 18, suggesting a correlation with the solvent's hydrodynamic nature.

Based on the presented results, it appears that if the ratio of the two critical volumes is equal to unity within experimental error, then the rotation of the solute is hydrodynamic; otherwise, it is non-hydrodynamic.

ACKNOWLEDGMENTS

J.S. and D.M. are grateful for the support from the Croatian Science Foundation under project nos. 1108 and 3168, and the Foundation of the Croatian Academy of Sciences and Arts. The work of doctoral student J.S. has been fully supported by the "Young researchers' career development project - training of doctoral students" of the Croatian Science Foundation. E.H. and M.P. gratefully acknowledge support from NSF MRI (grant No. 1626632) and NSF RUI (grant No. 1856746).

Supplemental Information

Coefficients B_{x0}, C_{x0}, B_{x2}, and C_{x2} for each RTIL and the relative permittivity values for RTILs.

TOC Graphic

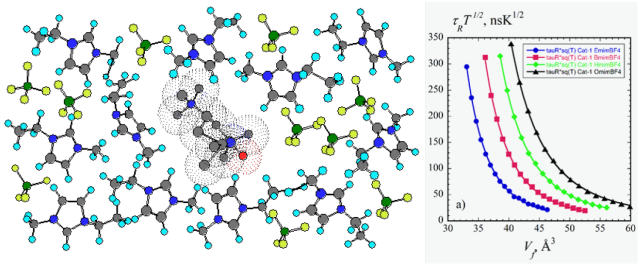

References

1. Kerton, F. M., *Alternative Solvents for Green Chemistry*; Cambridge, UK: RSC Pub.: Cambridge, UK, 2009.
2. Overbeck, V.; Ludwig, R., Chapter Three - NMR Studies of Protic Ionic Liquids. In *Annual Reports on NMR Spectroscopy*, Webb, G. A., Ed. Academic Press: 2018; Vol. 95, pp 147-190.
3. Pandey, S.; Baker, S. N.; Pandey, S.; Baker, G. A., Fluorescent Probe Studies of Polarity and Solvation within Room Temperature Ionic Liquids: A Review. *J. Fluoresc.* **2012**, *22*, 1313-1343.
4. Lei, Z.; Chen, B.; Koo, Y.-M.; MacFarlane, D. R., Introduction: Ionic Liquids. *Chem. Rev.* **2017**, *117*, 6633-6635.
5. Castner, E. W.; Wishart, J. F., Spotlight on Ionic Liquids. *J. Chem. Phys.* **2010**, *132*, 120901.
6. Patel, D. D.; Lee, J.-M., Applications of Ionic Liquids. *Chem. Rec.* **2012**, *12*, 329-355.
7. Wishart, J. F., Energy Applications of Ionic Liquids. *Energy Environ. Sci.* **2009**, *2*, 956-961.
8. Qureshi, Z. S.; Deshmukh, K. M.; Bhanage, B. M., Applications of Ionic Liquids in Organic Synthesis and Catalysis. *Clean Technol. Environ. Policy* **2014**, *16*, 1487-1513.
9. Han, D.; Row, K. H., Recent Applications of Ionic Liquids in Separation Technology. . *Molecules* **2010**, *15*, 2405-2426.
10. Carda–Broch, S.; Berthod, A.; Armstrong, D. W., Solvent Properties of the 1-Butyl-3-Methylimidazolium Hexafluorophosphate Ionic Liquid. *Anal. Bioanal. Chem.* **2003**, *375*, 191-199.
11. Plechkova, N. V.; Seddon, K. R., Applications of Ionic Liquids in the Chemical Industry. *Chem. Soc. Rev.* **2008**, *37*, 123-150.
12. Lawler, C.; Fayer, M. D., The Influence of Lithium Cations on Dynamics and Structure of Room Temperature Ionic Liquids. *J. Phys. Chem. B* **2013**, *117*, 9768-9774.
13. Fruchey, K.; Fayer, M. D., Dynamics in Organic Ionic Liquids in Distinct Regions Using Charged and Uncharged Orientational Relaxation Probes. *J. Phys. Chem. B* **2010**, *114*, 2840-2845.
14. Gangamallaiah, V.; Dutt, G. B., Effect of Alkyl Chain Length on the Rotational Diffusion of Nonpolar and Ionic Solutes in 1-Alkyl-3-Methylimidazolium-Bis(Trifluoromethylsulfonyl)Imides. *J. Phys Chem. B* **2013**, *117*, 12261-12267.
15. Akdogan, Y.; Heller, J.; Zimmermann, H.; Hinderberger, D., The Solvation of Nitroxide Radicals in Ionic Liquids Studied by High-Field Epr Spectroscopy. *Phys. Chem. Chem. Phys.* **2010**, *12*, 7874-7882.
16. Mladenova, B. Y.; Chumakova, N. A.; Pergushov, V. I.; Kokorin, A. I.; Grampp, G.; Kattnig, D. R., Rotational and Translational Diffusion of Spin Probes in Room-Temperature Ionic Liquids. *J. Phys. Chem. B* **2012**, *116*, 12295-12305.
17. Strehmel, V.; Berdzinski, S.; Rexhausen, H., Interactions between Ionic Liquids and Radicals. *J. Mol. Liq.* **2014**, *192*, 153-170.
18. Kaintz, A.; Baker, G.; Benesi, A.; Maroncelli, M., Solute Diffusion in Ionic Liquids, NMR Measurements and Comparisons to Conventional Solvents. *J. Phys. Chem. B* **2013**, *117*, 11697-11708.
19. Yasaka, Y.; Kimura, Y., Polarity and Nonpolarity of Ionic Liquids Viewed from the Rotational Dynamics of Carbon Monoxide. *J. Phys. Chem. B* **2015**, *119*, 15493-15501.
20. Rumble, C. A.; Kaintz, A.; Yadav, S. K.; Conway, B.; Araque, J. C.; Baker, G. A.; Margulis, C.; Maroncelli, M., Rotational Dynamics in Ionic Liquids from NMR Relaxation Experiments and Simulations: Benzene and 1-Ethyl-3-Methylimidazolium. *J. Phys. Chem. B* **2016**, *120*, 9450-9467.
21. Berliner, L. J., *Spin Labeling: Theory and Applications*. Academic Press: New York, 1976; Vol. 1.
22. Marsh, D., *Spin-Label Electron Paramagnetic Resonance Spectroscopy*; CRC Press: Boca Raton, 2020.
23. Noel, M. A. M.; Allendoerfer, R. D.; Osteryoung, R. A., Solvation in Ionic Liquids: An Epr Study. *J. Phys. Chem. A* **1992**, *96*, 2391-2394.
24. Miyake, Y.; Hidemori, T.; Akai, N.; Kawai, A.; Shibuya, K.; Koguchi, S.; Kitazume, T., Epr Study of Rotational Diffusion in Viscous Ionic Liquids: Analysis by a Fractional Stokes-Einstein-Debye Law. *Chem. Lett.* **2009**, *38*, 124-125.

25. Strehmel, V.; Laschewsky, A.; Stoesser, R.; Zehl, A.; Herrmann, W., Mobility of Spin Probes in Ionic Liquids. *J. Phys. Org. Chem.* **2006**, *19*, 318-325.
26. Evans, R. G.; Wain, A. J.; Hardacre, C.; Compton, R. G., An Electrochemical and ESR Spectroscopic Study on the Molecular Dynamics of Tempo in Room Temperature Ionic Liquid Solvents. *ChemPhysChem.* **2005**, *6*, 1035 –1039.
27. Stoesser, R.; Herrmann, W.; Zehl, A.; Laschewsky, A.; Strehmel, V., Microviscosity and Micropolarity Effects of Imidazolium Based Ionic Liquids Investigated by Spin Probes Their Diffusion and Spin Exchange. *Z. Phys. Chem.* **2006**, *220*, 1309-1342.
28. Akdogan, Y.; Junk, M. J. N.; Hinderberger, D., Effect of Ionic Liquids on the Solution Structure of Human Serum Albumin. *Biomacromolecules* **2011**, *12*, 1072-1079.
29. Merunka, D.; Peric, M., Measuring Radical Diffusion in Viscous Liquids by Electron Paramagnetic Resonance. *J. Mol. Liq.* **2019**, *277*, 886-894.
30. Merunka, D.; Peric, M., An Analysis of Radical Diffusion in Ionic Liquids in Terms of Free Volume Theory. *J. Chem. Phys.* **2020**, *152*.
31. Merunka, D.; Peric, M.; Peric, M., Study of Nanostructural Organization of Ionic Liquids by Electron Paramagnetic Resonance Spectroscopy. *J. Phys. Chem. B* **2015**, *119*, 3185-3193.
32. Mladenova, B. Y.; Kattnig, D. R.; Grampp, G. n., Room-Temperature Ionic Liquids Discerned Via Nitroxyl Spin Probe Dynamics. *J. Phys. Chem. B* **2011**, *115*, 8183-8198.
33. Kattnig, D. R.; Akdogan, Y.; Lieberwirth, I.; Hinderberger, D., Spin Probing of Supramolecular Structures in 1-Butyl-3-Methyl-Imidazolium Tetrafluoroborate/Water Mixtures. *Mol. Phys.* **2013**, *111*, 2723-2737.
34. Strehmel, V.; Rexhausen, H.; Strauch, P.; Strehmel, B., Temperature Dependence of Interactions between Stable Piperidine-1-Yloxyl Derivatives and a Semicrystalline Ionic Liquid. *ChemPhysChem.* **2010**, *11*, 2182-2190.
35. Stoesser, R.; Herrmann, W.; Zehl, A.; Strehmel, V.; Laschewsky, A., ESR Spin Probes in Ionic Liquids. *ChemPhysChem.* **2006**, *7*, 1106-1111.
36. Merunka, D.; Peric, M., Continuous Diffusion Model for Concentration Dependence of Nitroxide Epr Parameters in Normal and Supercooled Water. *J. Phys. Chem. B* **2017**, *121*, 5259-5272.
37. Halpern, H. J.; Peric, M.; Yu, C.; Bales, B. L., Rapid Quantitation of Parameters from Inhomogeneously Broadened Epr Spectra. *J. Magn. Reson. A* **1993**, *103*, 13-22.
38. Bales, B. L., Inhomogeneously Broadened Spin-Label Spectra. In *Spin Labeling: Theory and Applications*, Berliner, J. L.; Reuben, J., Eds. Plenum: New York, 1989; Vol. 8, pp 77-130.
39. Dobryakov, S. N.; Lebedev, Y. S., Analysis of Spectral Lines Whose Profile Is Described by a Composition of Gaussian and Lorentz Profiles. *Sov. Phys.* **1969**, *13*, 873-875.
40. Peric, I.; Merunka, D.; Bales, B. L.; Peric, M., Rotation of Four Small Nitroxide Probes in Supercooled Bulk Water. *J. Phys. Chem. Lett.* **2013**, *4*, 508-513.
41. Marsh, D., Experimental Methods in Spin-Label Spectral Analysis. In *Spin Labeling Theory and Applications*, Berliner, L. J.; Reuben, J., Eds. Plenum: New York, 1989; Vol. 8, pp 255-303.
42. Alves, M.; Bales, B. L.; Peric, M., Effect of Lysophosphatidylcholine on the Surface Hydration of Phospholipid Vesicles. *Biochim. Biophys. Acta* **2008**, *1778*, 414-422.
43. Goldman, S. A.; Bruno, G. V.; Polnaszek, C. F.; Freed, J. H., An ESR Study of Anisotropic Rotational Reorientation and Slow Tumbling in Liquid and Frozen Media. *J. Chem. Phys.* **1972**, *56*, 716-735.
44. Schreier, S.; Polnaszek, C. F.; Smith, I. C. P., Spin Labels in Membranes Problems in Practice. *Biochim. Biophys. Acta* **1978**, *515*, 375-436.
45. Speedy, R. J.; Angell, C. A., Isothermal Compressibility of Supercooled Water and Evidence for a Thermodynamic Singularity at -45°C. *J. Chem. Phys.* **1976**, *65*, 851-858.
46. McMillin, P. J.; Alegrete, M.; Peric, M.; Luchko, T., Electron Paramagnetic Resonance Measurements of Four Nitroxide Probes in Supercooled Water Explained by Molecular Dynamics Simulations. *J. Phys. Chem. B* **2020**, *124*, 3962-3972.

47. Götze, W., Recent Tests of the Mode-Coupling Theory for Glassy Dynamics. *J. Phys.: Condens. Matter* **1999**, *11*, A1-A45.
48. Götze, W.; Sjörgen, L., Relaxation Processes in Supercooled Liquids. *Rep. Prog. Phys.* **1992**, *55*, 241-376.
49. Qvist, J.; Mattea, C.; Sunde, E. P.; Halle, B., Rotational Dynamics in Supercooled Water from Nuclear Spin Relaxation and Molecular Simulations. *J. Chem. Phys.* **2012**, *136*, 204505.
50. Matthiesen, J.; Smith, R. S.; Kay, B. D., Mixing It Up: Measuring Diffusion in Supercooled Liquid Solutions of Methanol and Ethanol at Temperatures near the Glass Transition. *J. Phys. Chem. Lett.* **2011**, *2*, 557-561.
51. Rosa, A. C. P.; Vaveliuk, P.; Mundim, K. C.; Moret, M. A., A Model for Diffusive Systems: Beyond the Arrhenius Mechanism. *Physica A* **2016**, *450*, 317-322.
52. Struik, L. C. E., The Apparent Activation Energy for Mechanical and Dielectric Relaxation in Glass-Forming (Polymeric) Liquids: A Misconception? *Polymer* **1997**, *38*, 733-735.
53. Hayes, R.; Warr, G. G.; Atkin, R., Structure and Nanostructure in Ionic Liquids. *Chem. Rev.* **2015**, *115*, 6357-6426.
54. Canongia Lopes; José N. A.; Pádua, A. A. H., Nanostructural Organization in Ionic Liquids. *J. Phys. Chem. B* **2006**, *110*, 3330-3335.
55. Miyake, Y.; Akai, N.; Kawai, A.; Shibuya, K., Hydrodynamic Interpretation on the Rotational Diffusion of Peroxylamine Disulfonate Solute Dissolved in Room Temperature Ionic Liquids as Studied by Electron Paramagnetic Resonance Spectroscopy. *J. Phys. Chem. A* **2011**, *115*, 6347-6356.
56. Bondi, A., Van Der Waals Volumes and Radii. *J. Phys. Chem.* **1964**, *68*, 441-451.
57. Beichel, W.; Yu, Y.; Dlubek, G.; Krause-Rehberg, R.; Pionteck, J.; Pfefferkorn, D.; Bulut, S.; Bejan, D.; Friedrich, C.; Krossing, I., Free Volume in Ionic Liquids: A Connection of Experimentally Accessible Observables from PALS and PVT Experiments with the Molecular Structure from Xrd Data. *Phys. Chem. Chem. Phys.* **2013**, *15*, 8821-8830.
58. Zhao, Y. H.; Abraham, M. H.; Zissimos, A. M., Fast Calculation of Van Der Waals Volume as a Sum of Atomic and Bond Contributions and Its Application to Drug Compounds. *J. Org. Chem.* **2003**, *68*, 7368-7373.
59. Silva, W.; Zanatta, M.; Ferreira, A. S.; Corvo, M. C.; Cabrita, E. J., Revisiting Ionic Liquid Structure-Property Relationship: A Critical Analysis. *Int. J. Mol. Sci.* **2020**, *21*, 7745.
60. Frenkel, J., *Kinetic Theory of Liquids* Dover Publications Inc.: New York, 1955.
61. Doolittle, A. K., Studies in Newtonian Flow. Ii. The Dependence of the Viscosity of Liquids on Free-Space *J. Appl. Phys.* **1951**, *22*, 1471-1475.
62. Cohen, M. H.; Turnbull, D., Molecular Transposrt in Liquids and Glasses. *J. Chem. Phys.* **1959**, *31*, 1164-1169.
63. Turnbull, D.; Cohen, M. H., Free-Volume Model of the Amorphous Phase: Glass Transition. *J. Chem. Phys.* **1961**, *34*, 120-125.
64. Dlubek, G.; Yu, Y.; Krause-Rehberg, R.; Beichel, W.; Bulut, S.; Pogodina, N.; Krossing, I.; Friedrich, C., Free Volume in Imidazolium Triflimide ([C_3mim][Ntf_2]) Ionic Liquid from Positron Lifetime: Amorphous, Crystalline, and Liquid States. *J. Chem. Phys.* **2010**, *133*, 124502-9.
65. Yu, Y., et al., Free Volume and Phase Transitions of 1-Butyl-3-Methylimidazolium Based Ionic Liquids from Positron Lifetime Spectroscopy. *Phys. Chem. Chem. Phys.* **2012**, *14*, 6856-6868.
66. Yu, Y.; Bejan, D.; Krause-Rehberg, R., Free Volume Investigation of Imidazolium Ionic Liquids from Positron Lifetime Spectroscopy. *Fluid Phase Equilib.* **2014**, *363*, 48-54.
67. Bales, B. L.; Messina, L.; Vidal, A.; Peric, M.; Nascimento, O. R., Precision Relative Aggregation Number Determinations of Sds Micelles Using a Spin Probe. A Model of Micelle Surface Hydration. *J. Phys. Chem.* **1998**, *B 102*, 10347-10358.
68. Redfield, A. G., The Theory of Relaxation Processes. In *Advances in Magnetic and Optical Resonance*, Waugh, J. S., Ed. Academic Press: 1965; Vol. 1, pp 1-32.

69. Ottaviani, M. F.; Martini, G.; Nuti, L., Nitrogen Hyperfine Splitting of Nitroxide Solutions: Differently Structured and Charged Nitroxides as Probes of Environmental Properties. *Magn. Reson. Chem.* **1987**, *25*, 897-904.
70. Bullock, A. T.; Howard, C. B. J., Temperature-Dependent Hyperfine Coupling Constants in Electron Spin Resonance. Part 6. — Planar and Non-Planar Nitroxide Radicals *J. Chem. Soc., Faraday Trans. 1* **1980**, *76*, 1296–1300.
71. Lajzerowicz-Bonneteau, J., Molecular Structures of Nitroxides. In *Spin Labeling: Theory and Applications*, Berliner, J. L., Ed. Academic Press: New York, 1976; pp 239-249.
72. Singh, T.; Kumar, A., Static Dielectric Constant of Room Temperature Ionic Liquids: Internal Pressure and Cohesive Energy Density Approach. *J. Phys. Chem. B* **2008**, *112*, 12968-12972.
73. Padró, J. M.; Reta, M., Solvatochromic Parameters of Imidazolium-, Hydroxyammonium-, Pyridinium- and Phosphonium-Based Room Temperature Ionic Liquids. *J. Mol. Liq.* **2016**, *213*, 107-114.